

## Using gravitational waves to distinguish between neutron stars and black holes in compact binary mergers

STEPHANIE M. BROWN,<sup>1,2</sup> COLLIN D. CAPANO,<sup>1,2</sup> AND BADRI KRISHNAN<sup>1,2,3</sup>

<sup>1</sup>*Albert-Einstein-Institut, Max-Planck-Institut für Gravitationsphysik,  
Callinstraße 38, 30167 Hannover, Germany,*

<sup>2</sup>*Leibniz Universität Hannover, 30167 Hannover, Germany,*

<sup>3</sup>*Institute for Mathematics, Astrophysics and Particle Physics, Radboud University  
Heyendaalseweg 135, 6525 AJ Nijmegen, The Netherlands*

### ABSTRACT

In August 2017, the first detection of a binary neutron star merger, GW170817, made it possible to study neutron stars in compact binary systems using gravitational waves. Despite being the loudest (in terms of signal-to-noise ratio) gravitational wave detected to date, it was not possible to unequivocally determine that GW170817 was caused by the merger of two neutron stars instead of two black holes from the gravitational-wave data alone. That distinction was largely due to the accompanying electromagnetic counterpart. This raises the question: under what circumstances can gravitational-wave data alone, in the absence of an electromagnetic signal, be used to distinguish between different types of mergers? Here, we study whether a neutron-star–black-hole binary merger can be distinguished from a binary black hole merger using gravitational-wave data alone. We build on earlier results using chiral effective field theory to explore whether the data from LIGO and Virgo, LIGO A+, LIGO Voyager, or Cosmic Explorer could lead to such a distinction. The results suggest that the present LIGO-Virgo detector network will most likely be unable to distinguish between these systems even with the planned near-term upgrades. However, given an event with favorable parameters, third-generation instruments such as Cosmic Explorer will be capable of making this distinction. This result further strengthens the science case for third-generation detectors.

### 1. INTRODUCTION

Neutron stars are unique laboratories for studying ultra-dense, relativistic matter. Multimessenger observations of neutron star mergers provide unique opportunities to extract relevant physical information (such as compactness) from them. Measurements of neutron star compactness and radii are vital to constraining the equation of state of ultra-dense matter [Lattimer & Prakash \(2001\)](#). In addition to the observation of the neutron star mergers GW170817 and GW190425 [Abbott et al. \(2017, 2020\)](#), X-ray observations of accreting neutron stars [Özel & Freire \(2016\)](#); [Watts et al. \(2016\)](#) have placed constraints on neutron star mass and radii. Of these, the recent results from NICER are especially promising [Bogdanov et al. \(2019a,b\)](#); [Raaijmakers et al. \(2020\)](#). These studies typically constrain the radii to a range of 10–14 km.

The observation of GW170817 and its electromagnetic counterpart led to several important advances. The detection of the electromagnetic counterpart was made possible by the fact that the LIGO-Virgo observation constrained the sky location of the event to 28 deg<sup>2</sup>. It was the detection of gamma-ray burst GRB170817A 1.7 seconds after GW170817 that provided the initial evidence that this event contained neutron star matter. Transient electromagnetic follow-ups [Soares-Santos et al. \(2017\)](#); [Cantiello et al. \(2018\)](#) further supported the neutron star hypothesis and provided more information about the binary. The combination of electromagnetic and gravitational wave observations led to new constraints on neutron star physics. For instance, an analysis of GW170817 placed an upper limit of  $11.0_{-0.6}^{+0.9}$  km on the radius of a  $1.4 M_{\odot}$  neutron star [Capano et al. \(2020\)](#).

Though GW170817 led to new constraints on the radius and tidal deformability of neutron stars, it alone was not sufficient to determine that the event was a binary neutron star rather than a binary black hole. The evidence that this was a binary neutron star merger came from observations of the electromagnetic counterpart. In future observations, we will likely not be in the fortuitous position of having a clear electromagnetic counterpart. This leads to the question: under what conditions can a gravitational wave signal alone differentiate between a binary neutron star and a binary black hole? Similarly, can a neutron-star–black-hole binary be differentiated from a binary black hole by gravitational wave observations alone? In this work, we address the second of these questions for current and future gravitational wave detectors. Current detectors may not be able to successfully differentiate between neutron-star–black-hole binaries and binary black holes, making future detectors vitally important.

In addition to the current LIGO-Virgo detectors, we consider LIGO A+, LIGO Voyager, and Cosmic Explorer. The plans for LIGO A+ aim to improve the detection range of binary neutron stars at  $1.4 M_{\odot}$  by a factor of 1.9 [Barsotti et al. \(2018\)](#). These improvements to LIGO may occur as soon as three years from now. Further plans exist for LIGO Voyager, which will further increase detector sensitivity [McClelland et al. \(2016\)](#). Power spectral density curves for the design sensitivity of these two detectors are publicly available [Evans et al. \(2020\)](#) and are used in our analysis. Beyond LIGO A+ and LIGO Voyager, there are plans for third-generation (3G) detectors such as Cosmic Explorer. We consider both Cosmic Explorer’s first run (CE1) expected to take place in the 2030s and its second run (CE2) which is planned for the 2040s. Cosmic Explorer is expected to vastly expand the number of neutron stars detected by expanding the redshift horizon out to 3.1 in the first run. With predicted signal-to-noise ratios going up by an order of magnitude for nearby sources, Cosmic Explorer will greatly improve our tidal deformability measurements [Reitze et al. \(2019\)](#).

We use standard Bayesian model selection tools in our analysis. The evidences are calculated using dynamic nested sampling package DYNesty [Speagle \(2020\)](#) accessed through the PyCBC toolkit [Biver et al. \(2019\)](#). In this analysis, we employ neutron star equations of state derived from chiral effective field theory, a theory that uses an effective description of nuclear matter in terms of nucleons and pions [Weinberg \(1990, 1991\)](#); [Machleidt & Entem \(2011\)](#); [Epelbaum et al. \(2009\)](#). The chiral effective field theory framework not only leads to equations of state consistent with all symmetries of the strong interactions and known experimental constraints, but it also provides reliable uncertainty estimates. We use the same subset of the equations of state employed successfully in [Capano et al. \(2020\)](#) to improve constraints on neutron star radii.

We show that, at least for the proposed gravitational wave detectors within the next decade (namely LIGO A+ and Voyager), it is very unlikely that gravitational wave observations alone will be able to distinguish neutron-star–black-hole binaries from binary black holes. Third-generation of gravitational wave detectors will be required for this purpose. Sec. 2 details our model selection procedure, Sec. 3 presents the main results, and Sec. 4 concludes with a discussion of the implication of these results.

## 2. METHODS

Consider a network of gravitational wave detectors, and let  $d_i(t)$  denote the gravitational wave strain time series data in the  $i^{\text{th}}$  detector as a function of time  $t$ . The collection of all time series in the network will be denoted  $\vec{d}$ . The data is the sum of detector noise  $n_i(t)$  and a possible astrophysical signal  $h(t)$  which depends on certain parameters which we collectively denote  $\vec{\vartheta}$ :

$$d_i(t) = n_i(t) + h_i(t; \vec{\vartheta}). \quad (1)$$

The central goal of a Bayesian analysis is to calculate the posterior probability distributions  $p(\vec{\vartheta} | \vec{d}(t))$  of the parameters  $\vec{\vartheta}$ . The basis of this is Bayes’ Theorem

$$p(\vec{\vartheta} | \vec{d}(t), H) = \frac{p(\vec{d}(t) | \vec{\vartheta}, H) p(\vec{\vartheta} | H)}{p(\vec{d}(t) | H)}. \quad (2)$$

The fourteen parameters appearing in  $\vec{\vartheta}$  are discussed below. The prior,  $p(\vec{\vartheta} | H)$ , represents the knowledge that we have about the parameters before considering the data. The likelihood function,  $p(\vec{d}(t) | \vec{\vartheta}, H)$ , is the probability of obtaining the observation,  $\vec{d}(t)$ , given a waveform  $H$  with parameters  $\vec{\vartheta}$ .

In order to obtain a posterior distribution on one or a few parameters, we marginalize over the other parameters by integrating  $p(\vec{d}(t) | \vec{\vartheta}, H) p(\vec{\vartheta} | H)$ . Marginalizing over all parameters yields the evidence. Comparing the evidence ( $p(\vec{d}(t) | H)$ ) of two different models ( $H_A$  and  $H_B$ ) gives the Bayes factor,

$$\mathcal{B} = \frac{p(\vec{d}(t) | H_A)}{p(\vec{d}(t) | H_B)}. \quad (3)$$

This number indicates how much the data supports one model versus the other. When  $\mathcal{B} > 1$ ,  $H_A$  is favored over  $H_B$ ; the larger  $\mathcal{B}$  is, the more  $H_A$  is favored. In this study, the Bayes Factors reported give how much  $A$ , neutron-star–black-hole model, is favored over  $B$ , the binary black hole model. We measure evidences using the dynamic nested sampling package DYNesty [Speagle \(2020\)](#). To crosscheck our results, we analyze a subset of our signals using a parallel-tempered version of the emcee Markov Chain Monte Carlo sampler [Vousden et al. \(2015\)](#); [Foreman-Mackey et al. \(2013\)](#). The resulting posteriors were consistent with those generated by DYNesty.

We generate simulated gravitational waves from neutron-star–black-hole binary (NSBH) mergers, and add these to simulated Gaussian noise colored by the power spectral density (PSD) of the target detector configuration. Gravitational waves from NSBH mergers depend on a number of variables  $\vec{\vartheta}$ . The most relevant parameters for this work are the component masses  $m_{1,2}$  and the tidal deformabilities  $\Lambda_{1,2}$ , defined as

$$\Lambda_{1,2} = \frac{2k_2}{3} \left( \frac{c^2 R_{1,2}}{Gm_{1,2}} \right)^5. \quad (4)$$

Here  $R_{1,2}$  are the radii of the individual stars, and  $k_2$  is the tidal Love number which is determined from the equation of state and the mass. The leading order effect of  $\Lambda_{1,2}$  on the waveform is through the combined tidal deformability parameter

$$\tilde{\Lambda} = \frac{16}{13} \frac{(12q + 1)\Lambda_1 + (12 + q)q^4\Lambda_2}{(1 + q)^5}, \quad (5)$$

where we define the mass ratio  $q = m_2/m_1 \geq 1$ . The tidal deformability is the primary means to distinguish black holes from neutron stars using gravitational waves and to infer the equation of state of neutron stars. By definition, a black hole has zero tidal deformability, while larger values of  $\Lambda$  correspond to stiffer equations of state.

As the binary inspirals, merges, and then settles into a stable black hole, it emits gravitational waves. Gravitational waves have two polarizations, denoted as  $h_{+,\times}$ . The intrinsic parameters affect the phase evolution of the gravitational waves. Some parameters, such as the chirp mass and symmetric mass ratio, also affect the amplitude of the gravitational wave. The symmetric mass ratio  $\nu$  and chirp mass  $\mathcal{M}$  are defined respectively as

$$\nu = \frac{m_1 m_2}{(m_1 + m_2)^2}, \quad \mathcal{M} = \mu^{3/5} M^{2/5} \quad (6)$$

In the source frame, say one aligned with the source axis,  $h_{+,\times}$  depend on the direction to the detector; equivalently, in a geocentric frame,  $h_{+,\times}$  depend on the orientation of the source. Furthermore, the detectors do not detect  $h_+$  and  $h_\times$  directly, they detect the gravitational wave strain:

$$h(t) = F_+(t; \alpha, \delta, \psi)h_+ + F_\times(t; \alpha, \delta, \psi)h_\times \quad (7)$$

where  $F_+$  and  $F_\times$  are functions of the angles defining the location of the source. These are typically expressed as sky location (right ascension:  $\alpha$ , declination:  $\delta$ ) and polarization angle  $\psi$ . Additionally, the amplitude depends on the inclination angle  $\iota$  and luminosity distance of the source. These extrinsic variables affect only the amplitude of the gravitational waveform. The last variable that defines the detected strain is the detection time  $t_c$  (which determines the detector position and orientation).

The waveforms are obtained by injecting the parameters into the PyCBC toolkit [Biver et al. \(2019\)](#). The injection generates a gravitational waveform using parameters  $\vec{\vartheta}$  and a waveform approximant. We use a waveform approximant that combines inspiral, merger, and ringdown portions of the signal and has been calibrated to numerical relativity results (see e.g. [Ajith et al. \(2008\)](#); [Buonanno & Damour \(1999\)](#); [Damour & Nagar \(2010\)](#); [Pannarale et al. \(2013\)](#); [Lackey et al. \(2014\)](#)). The particular waveform model used in this work is IMRPhenomD\_NRTidal [Khan et al. \(2016\)](#); [Husa et al. \(2016\)](#); [Dietrich et al. \(2017, 2019\)](#). [Capano et al. \(2020\)](#) demonstrated that due to waveform systematics at high signal-to-noise ratios, PhenomDNRT constrained neutron star tidal deformability better than TaylorF2. For this reason, we choose to use the IMRPhenomD\_NRTidal model. For the data analysis, colored Gaussian noise is added to the injected waveform using the detector power spectral density curve.

We set the neutron star mass to the standard  $1.4M_\odot$  and vary the mass of the black hole between  $(5, 10, 15, 20)M_\odot$  and the distance between  $(40, 80)$  Mpc. For the neutron star, we used two of the equations of state that were favored by previous parameter estimation using chiral effective field theory [Capano et al. \(2020\)](#). The first of these equations is the maximum likelihood equation of state found in [Capano et al. \(2020\)](#). However, this equation of state is quite soft and leads to small tidal deformabilities. As neutron stars with large tidal deformabilities would be easier to distinguish from a black hole, we also test a stiff equation of state. The equation of state is the stiffest equation of state in the 90th percentile credible interval of [Capano et al. \(2020\)](#).

For both the injection and the parameter estimation, the sky location is fixed to the reported sky location of GW170817 [Soares-Santos et al. \(2017\)](#):

$$\alpha = 13^{\text{h}} 09^{\text{m}} 48.1^{\text{s}}, \quad \delta = -23^\circ 22' 53.4'' . \quad (8)$$

For the injection, the polarization, inclination, and coalescence time are set to

$$\Psi = \pi, \quad t_c = 1187008882.4434, \quad \iota = 0.35 . \quad (9)$$

For the analysis with DYNESTY, we set up the parameter estimation to be as similar to the analysis for GW170817 as possible. As was done for GW170817 [Capano et al. \(2020\)](#); [De et al. \(2018\)](#), we fix the sky location and distance. The variable parameters in our parameter estimation were the individual masses, spins, coalescence time, inclination, and polarization. The prior for the neutron star mass object is uniform on  $[1M_\odot, 2M_\odot]$  and for the black hole it was uniform on  $[m_{BH} - 2, m_{BH} + 2]$ . The spin priors were both low spin  $[-0.05, 0.05]$ , which has been used in previous analyses of GW170817 (see e.g. [Capano et al. \(2020\)](#); [De et al. \(2018\)](#); [Abbott et al. \(2017\)](#)). We constrain the inclination and polarization angles to be between 0 and  $2\pi$  rad, and the coalescence time is assumed to be in the range  $t_c \pm 0.1$  sec.

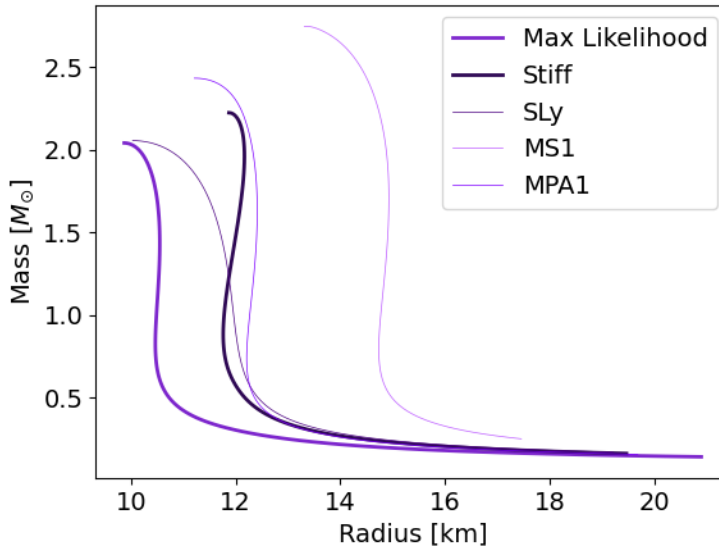


**Figure 1.** Mass radius curves for the two equations of state used in this analysis compared to a three commonly used equations of state. The two equations used here are labelled as ‘stiff’ and ‘maximum likelihood’ respectively.

The tidal deformability parameter estimation is what differs between our two models. To test the binary black hole hypothesis, the tidal deformability of both objects is set to 0 in the parameter estimation. For the neutron-star–black-hole model parameter estimation, we looked at two cases. In one case, we sampled over the equation of state for the neutron star mass object. The equation of state has a uniform prior in radius at  $1.4M_{\odot}$ , and there are 2,000 equations in the prior. The equation selected was then used to calculate the tidal deformability given  $m_1$  and  $m_2$ . In the other case, we set the equation of state as a static variable in the parameter estimation. The reason for this is that, while the nuclear equation of state is currently not well constrained, it is expected that experiments such as NICER will greatly improve our knowledge over the next decade. To take this into account, we consider the extreme case: the one in which the equation of state is known exactly and is thus fixed in the parameter estimation.

### 3. RESULTS

In order to determine if the gravitational waves can distinguish between neutron-star–black-holes and binary black holes, we look at the  $\ln$  Bayes factor ( $\log_e \mathcal{B}$ ) between two models. There is much debate on what constitutes evidence, strong evidence, decisive evidence, and so on. Commonly cited statistics papers such as [Kass & Raferty \(1995\)](#) state that  $\log_{10} \mathcal{B} \geq 2$  ( $\log_e \mathcal{B} \geq 5$ ) can be considered decisive evidence in favor of a model. However, this has been called into question for gravitational wave model selection because of the high dimensionality and complexity of the parameter space. Additionally, we found that using different sampler settings and different noise realizations that the  $\ln \mathcal{B}$  could vary about  $\pm 1$  at the  $1\sigma$  level when  $\ln \mathcal{B} \approx 3$  and around  $\pm 2, 3$  when  $\ln \mathcal{B} \approx 10$ . Taking these things into consideration, we have decided to require a higher threshold. This higher cut-off ensures that our conclusions remain conservative regarding the capabilities of the gravitational wave detectors that we consider. We require

$$\log_e \mathcal{B} \geq 10 \tag{10}$$

for decisive evidence.

The errors quoted in this paper are based on the standard deviation of  $\ln \mathcal{B}$  across instances of the same injection parameters but with different noise realizations. Except for the specific case of  $m_{BH} = 5M_{\odot}$ , the error for the current LIGO-Virgo detector network, LIGO A+, and LIGO Voyager is  $< 1$ , and for Cosmic Explorer 1 and 2, the error is  $< 2.5$ . The errors in the case of  $m_{BH} = 5M_{\odot}$  are larger (for details see Table 11). The maximum error for the current LIGO-Virgo detector network is  $\approx 1.3$ . This increases to 1.5 for LIGO A+, 3.1 for LIGO Voyager,  $\approx 13$  for Cosmic Explorer 1 and  $\approx 19$  for Cosmic Explorer 2. The absolute values of the errors increase as the detectors improve and the signal-to-noise ratio increases, which seems counter-intuitive at first glance. However, as one would expect, the fractional error actually decreases as Bayes factors and signal-to-noise ratios increase. As mentioned above these larger errors are part of the reason why a conservative cut-off criterion was chosen.

As mentioned earlier, we shall present results for a  $1.4M_{\odot}$  neutron star with a black hole companion on mass  $(5, 10, 15, 20)M_{\odot}$ , and we shall take the distance to be 40 or 80 Mpc. The neutron star equation of state shall be either of the ones shown in Fig. 1. We shall consider the following detector networks:

- The current LIGO-Virgo Network at design sensitivity in the zero-detuned high power configuration [LIGO Scientific Collaboration \(2018\)](#)
- The LIGO A+ upgrade [Evans et al. \(2020\)](#).
- LIGO Voyager [Evans et al. \(2020\)](#).
- The first observational run of the proposed 40 km Cosmic Explorer detector in the “compact binary” configuration [Srivastava et al. \(2020\)](#).
- The second observational run of the 40 km Cosmic Explorer detector, again in the “compact binary” configuration [Srivastava et al. \(2020\)](#).

The results of our analysis for the various combinations of masses, distances and detector network are shown in Figs. 2, 3 and 4, and in Tables 1-10.

The Figs. 2 and 3 show the Bayes factors for the  $5M_{\odot}$  and  $10M_{\odot}$  black hole cases respectively. As expected, the  $5M_{\odot}$  leads to larger Bayes factors since the tidal effects on the neutron star are more significant. Nevertheless, for both cases, the important observation for our purposes is that the Bayes factors exceed our chosen threshold of Eq. 10 only for the third-generation Cosmic Explorer detectors. The Voyager results in Fig. 2 do come close to the threshold, but the variation is seen to be large. The Bayes factor would easily be reduced if the system were further away, as is very likely. This same conclusion is evident in Fig. 4 which shows all the combinations that we have considered:  $\log_e \mathcal{B} > 10$  only for the third-generation detectors.

The precise numerical values for the Bayes factors are found in the Tables 1-10. Looking at Tables 1 and 2, we see that for the current LIGO-Virgo detector network  $|\log_e \mathcal{B}| < 1$  in all cases. For the upgraded detector LIGO A+, the range of Bayes factors is  $[0.0, 2.5]$  for the variable equation of state analysis and  $[-0.3, 3.2]$  for the constant equation of state analysis. From Tables 3 and 4, we see that except for the  $5M_{\odot}$  black hole companion and the 90<sup>th</sup> percentile stiff equation of state all  $|\log_e \mathcal{B}| < 1$ . We also see that the largest Bayes factor occurs, as expected, for the 90<sup>th</sup> percentile stiff equation of state with a  $5M_{\odot}$  black hole at 40Mpc. With the LIGO Voyager, we once again see the highest Bayes factor for the  $5M_{\odot}$  black hole companion and the stiff equation of state at 40Mpc. In this case, we have 8.7 for the variable equation of state case and 9.5 for the constant equation of state case. Excluding these values, the range of  $\log_e \mathcal{B}$  is  $[-0.4, 2.0]$  for the variable equation of state and  $[-0.7, 2.4]$  for the constant equation of state case.

The results of parameter estimation using the third-generation Cosmic Explorer 1 and Cosmic Explorer 2 are more optimistic. We finally see values well above the threshold of 10. Looking at Tables 7 and 8, we see that for Cosmic Explorer 1, there are now three instances for both the variable and constant equation of state cases that well exceed our Bayes factor threshold. In all cases, this occurs for a black hole companion of mass  $5M_{\odot}$ . For the stiff equation of state we have  $\log_e \mathcal{B}$  of (93.9, 95.4) at 40Mpc and (21.9, 22.5) at 80Mpc for the (variable, constant) equation of state cases. Additionally, for the maximum likelihood equation of state, at 40Mpc, we have  $\log_e \mathcal{B}$  of (16.8, 17.7) for the variable and constant equation of state respectively. In Tables 9 and 10, it can be seen that the results of CE2 are very similar to those of CE1. We have  $\log_e \mathcal{B} > 10$  for cases with a low black hole mass, for both equations of state, out to 80Mpc for the stiff equation of state and 40Mpc in the maximum likelihood case.

#### 4. DISCUSSION

The results demonstrate that the current LIGO and Virgo detectors are not sufficient to differentiate between neutron-star–black-hole and binary black hole systems. In fact, the success of the A+ and Voyager is dubious. There were no cases for any of these three detectors where the  $\ln \mathcal{B}$  exceeded our threshold. However, it is important to note that the cases with the highest  $\ln \mathcal{B}$  always occur with the stiff equation of state, the  $5M_{\odot}$  black hole companion, and at 40Mpc. This is not surprising. The stiff equation of state was selected specifically for this property and the signal-to-noise ratio at 40Mpc is higher than at 80Mpc.

It can be seen that the ability to differentiate between a neutron-star–black-hole system and a binary black hole system does not directly correspond directly to the signal-to-noise ratio. The highest  $\ln \mathcal{B}$  occurs for  $m_{BH} = 5M_{\odot}$ , even though systems with  $m_{BH} = 10, 15, 20M_{\odot}$  have higher signal-to-noise ratios. The tidal effects decrease as mass increases and this effect is clearly of greater importance than the increase in signal strength. Detection of a neutron-star–black-hole with a low mass ratio will almost certainly be required to give evidence of neutron star matter in the gravitational wave signal. Additionally, the nuclear equation

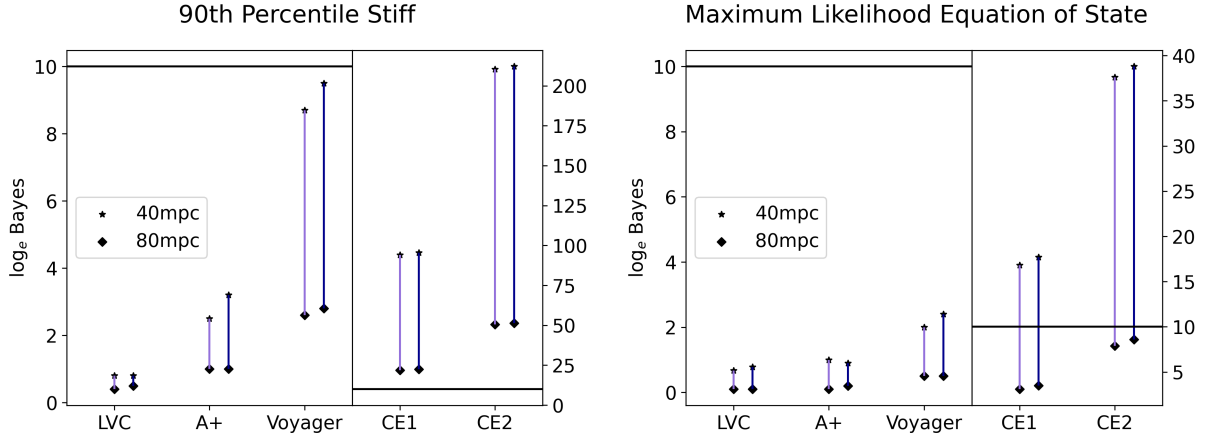


**Figure 2.**  $\log_e \mathcal{B}$  for each detector with  $M_{BH} = 5M_\odot$ . The vertical line spans the range of Bayes factors for a given detector with the purple line on the left indicates a variable equation of state run and the blue line on the right indicates a constant equation of state. The horizontal black line corresponds to the  $\log_e \mathcal{B} = 10$  cut-off. Since the Cosmic Explorer 1 and 2 runs have a significantly high Bayes factors, the plots are split with different y-axis for current and third-generation detectors.

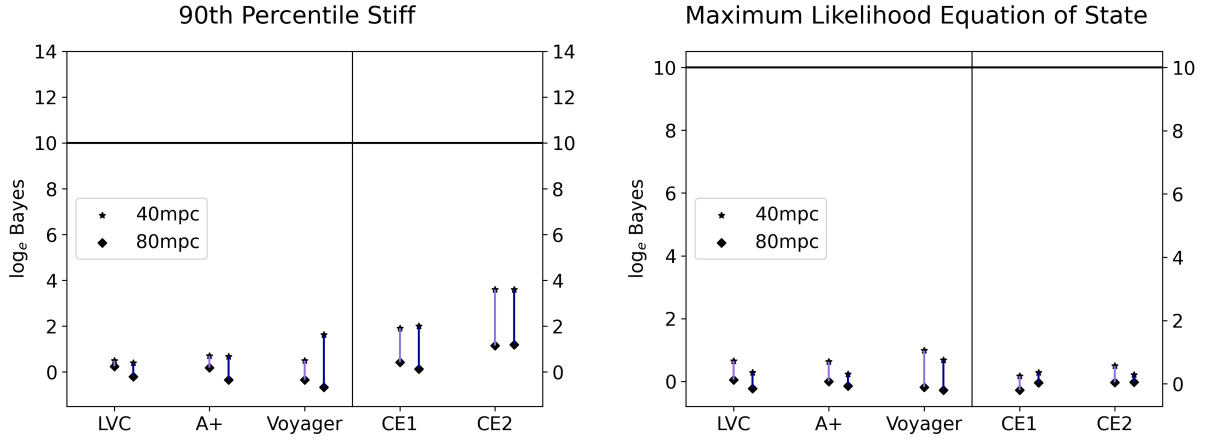


**Figure 3.**  $\log_e \mathcal{B}$  for each detector with  $M_{BH} = 10M_\odot$ . The vertical line spans the range of Bayes factors for a given detector with the purple line on the left indicating a variable equation of state run and the blue line on the right indicating a constant equation of state. The horizontal black line corresponds to the  $\log_e \mathcal{B} = 10$  cut-off.

of state itself is an important factor in how soon and how likely we are to be able to distinguish a neutron-star–black-hole system from a binary black hole system.

When looking at LIGO Voyager, we saw that in one case the results were close to our cut-off. Keep in mind, however, that this analysis was done with design sensitivity curves and this result occurs only for the fine-tuned case of a very close binary with a very small black hole that has a rather stiff equation of state. Despite LIGO-Virgo’s recent detection of an object in the mass gap,  $5M_\odot$  is still firmly on the low end of what we expect for black hole masses. Looking at Figure 3, it’s obvious that, when the companion mass increases to even  $10M_\odot$ , the Bayes factor drops rapidly regardless of distance or equation of state for these detectors. If the equation of state is as soft as the analysis of GW170817 suggests, then LIGO Voyager will certainly be unable to distinguish neutron-star–black-hole systems from binary black holes no matter how close or loud the signal is.

It is extremely likely that 3G detectors will be required to obtain decisive evidence of neutron-star–black-hole from gravitational wave data. We see here that the proposed design for Cosmic Explorer may very well allow for these detections. Looking at Figure 2 and Table 7, we see that regardless of the nuclear equation of state, there are systems which have  $\ln \mathcal{B} > 10$ . Thus, if current analyses of GW170817 are accurate, we will be waiting until Cosmic Explorer for gravitational wave evidence of neutron-star–black-hole systems. Additionally Cosmic Explorer 1 seems to be able to do this measurement at distances out 80 Mpc (stiff equation of state), which expands the number of candidate systems greatly. Clearly, even with very sensitive future detectors, the

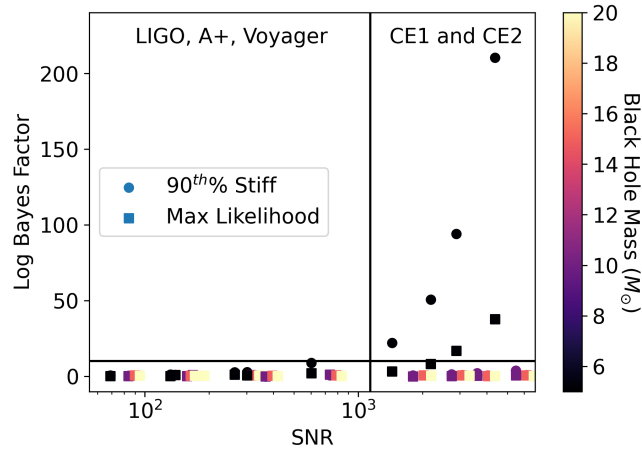


**Figure 4.**  $\log_e$  Bayes Factor for all combinations of parameters and detectors as a function of the signal-to-noise ratio. The marker color indicates the mass of the black hole in the system. The black horizontal line shows the cut-off of  $\log_e \mathcal{B} = 10$ . The vertical line indicates the shift from current detectors (left) to third-generation detectors (right).

ability to distinguish neutron-star–black-hole systems from binary black holes is very dependent on the mass of the black hole in the binary.

## REFERENCES

- Abbott, B., Abbott, R., Abbott, T., et al. 2017, *Physical Review Letters*, 119, 161101, doi: [10.1103/physrevlett.119.161101](https://doi.org/10.1103/physrevlett.119.161101)
- Abbott, B. P., Abbott, R., Abbott, T. D., et al. 2020, *The Astrophysical Journal*, 892, L3, doi: [10.3847/2041-8213/ab75f5](https://doi.org/10.3847/2041-8213/ab75f5)
- AEI. 2017, The Atlas Computing Cluster, <https://www.aei.mpg.de/43564/atlas-computing-cluster>, <https://www.aei.mpg.de/43564/atlas-computing-cluster>
- Ajith, P., Babak, S., Chen, Y., et al. 2008, *Phys. Rev. D.*, 77, 104017, doi: [10.1103/PhysRevD.77.104017](https://doi.org/10.1103/PhysRevD.77.104017)
- Barsotti, L., McCuller, L., Evans, M., & Fritschel, F. 2018, The A+ design curve, Tech. Rep. T1500293-v12, LIGO Scientific Collaboration. <https://dcc.ligo.org/LIGO-T1800042/public>
- Biwer, C. M., Capano, C. D., De, S., et al. 2019, *Publications of the Astronomical Society of the Pacific*, 131, 024503, doi: [10.1088/1538-3873/aaef0b](https://doi.org/10.1088/1538-3873/aaef0b)
- Bogdanov, S., Guillot, S., Ray, P. S., et al. 2019a, *The Astrophysical Journal*, 887, L25, doi: [10.3847/2041-8213/ab53eb](https://doi.org/10.3847/2041-8213/ab53eb)
- Bogdanov, S., Lamb, F. K., Mahmoodifar, S., et al. 2019b, *The Astrophysical Journal*, 887, L26, doi: [10.3847/2041-8213/ab5968](https://doi.org/10.3847/2041-8213/ab5968)
- Buonanno, A., & Damour, T. 1999, *Physical Review D*, 59, 084006, doi: [10.1103/physrevd.59.084006](https://doi.org/10.1103/physrevd.59.084006)
- Cantiello, M., Jensen, J. B., Blakeslee, J. P., et al. 2018, *The Astrophysical Journal*, 854, L31, doi: [10.3847/2041-8213/aaad64](https://doi.org/10.3847/2041-8213/aaad64)
- Capano, C. D., Tews, I., Brown, S. M., et al. 2020, *Nature Astronomy*, 4, 625–632, doi: [10.1038/s41550-020-1014-6](https://doi.org/10.1038/s41550-020-1014-6)
- Damour, T., & Nagar, A. 2010, *Physical Review D*, 81, 084016, doi: [10.1103/physrevd.81.084016](https://doi.org/10.1103/physrevd.81.084016)
- De, S., Finstad, D., Lattimer, J. M., et al. 2018, *Physical Review Letters*, 121, 091102, doi: [10.1103/physrevlett.121.091102](https://doi.org/10.1103/physrevlett.121.091102)
- Dietrich, T., Bernuzzi, S., & Tichy, W. 2017, *Physical Review D*, 96, 121501, doi: [10.1103/physrevd.96.121501](https://doi.org/10.1103/physrevd.96.121501)
- Dietrich, T., Khan, S., Dudi, R., et al. 2019, *Physical Review D*, 99, 024029, doi: [10.1103/physrevd.99.024029](https://doi.org/10.1103/physrevd.99.024029)
- Epelbaum, E., Hammer, H.-W., & Meißner, U.-G. 2009, *Reviews of Modern Physics*, 81, 1773–1825, doi: [10.1103/revmodphys.81.1773](https://doi.org/10.1103/revmodphys.81.1773)
- Evans, M., Sturani, R., Vitale, S., & Hall, E. 2020, Unofficial sensitivity curves (ASD) for aLIGO, Kagra, Virgo, Voyager, Cosmic Explorer and ET, Tech. Rep. T1500293-v12, LIGO Scientific Collaboration. <https://dcc.ligo.org/LIGO-T1500293-v12/public>
- Foreman-Mackey, D., Hogg, D. W., Lang, D., & Goodman, J. 2013, *Publ. Astron. Soc. Pac.*, 125, 306–312, doi: [10.1086/670067](https://doi.org/10.1086/670067)
- Husa, S., Khan, S., Hannam, M., et al. 2016, *Physical Review D*, 93, 044006, doi: [10.1103/physrevd.93.044006](https://doi.org/10.1103/physrevd.93.044006)
- Kass, R. E., & Raferty, A. E. 1995, *Journal of the American Statistical Association*, 90, 773, doi: [10.2307/2291091](https://doi.org/10.2307/2291091)

- Khan, S., Husa, S., Hannam, M., et al. 2016, *Physical Review D*, 93, 044007, doi: [10.1103/physrevd.93.044007](https://doi.org/10.1103/physrevd.93.044007)
- Lackey, B. D., Kyutoku, K., Shibata, M., Brady, P. R., & Friedman, J. L. 2014, *Physical Review D*, 89, 043009, doi: [10.1103/physrevd.89.043009](https://doi.org/10.1103/physrevd.89.043009)
- Lattimer, J. M., & Prakash, M. 2001, *The Astrophysical Journal*, 550, 426–442, doi: [10.1086/319702](https://doi.org/10.1086/319702)
- LIGO Scientific Collaboration. 2018, LIGO Algorithm Library - LALSuite, free software (GPL), doi: [10.7935/GT1W-FZ16](https://doi.org/10.7935/GT1W-FZ16)
- Machleidt, R., & Entem, D. 2011, *Physics Reports*, 503, 1–75, doi: [10.1016/j.physrep.2011.02.001](https://doi.org/10.1016/j.physrep.2011.02.001)
- McClelland, D., Cavaglia, M., Evans, M., et al. 2016, *The LSC-Virgo White Paper on Instrument Science (2016-2017 edition)*, Tech. Rep. LIGO-T1600119–v4, LIGO Scientific Collaboration. <https://dcc.ligo.org/LIGO-T1600119/public>
- Pannarale, F., Berti, E., Kyutoku, K., & Shibata, M. 2013, *Physical Review D*, 88, 084011, doi: [10.1103/physrevd.88.084011](https://doi.org/10.1103/physrevd.88.084011)
- Raaijmakers, G., Greif, S. K., Riley, T. E., et al. 2020, *The Astrophysical Journal*, 893, L21, doi: [10.3847/2041-8213/ab822f](https://doi.org/10.3847/2041-8213/ab822f)
- Reitze, D., Adhikari, R. X., Ballmer, S., et al. 2019, *Cosmic Explorer: The U.S. Contribution to Gravitational-Wave Astronomy beyond LIGO*. <https://arxiv.org/abs/1907.04833>
- Soares-Santos, M., Holz, D. E., Annis, J., et al. 2017, *The Astrophysical Journal*, 848, L16, doi: [10.3847/2041-8213/aa9059](https://doi.org/10.3847/2041-8213/aa9059)
- Speagle, J. S. 2020, *Monthly Notices of the Royal Astronomical Society*, 493, 3132–3158, doi: [10.1093/mnras/staa278](https://doi.org/10.1093/mnras/staa278)
- Srivastava, V., Kuns, K., Hall, E., Ballmer, S., & Evans, M. 2020, *Sensitivity Curves for the Cosmic Explorer Trade Study*, Tech. Rep. CE-T2000007–v2, Cosmic Explorer. <https://dcc.cosmicexplorer.org/CE-T2000007-v2>
- Vousden, W. D., Farr, W. M., & Mandel, I. 2015, *Monthly Notices of the Royal Astronomical Society*, 455, 1919, doi: [10.1093/mnras/stv2422](https://doi.org/10.1093/mnras/stv2422)
- Watts, A. L., Andersson, N., Chakrabarty, D., et al. 2016, *Reviews of Modern Physics*, 88, doi: [10.1103/revmodphys.88.021001](https://doi.org/10.1103/revmodphys.88.021001)
- Weinberg, S. 1990, *Physics Letters B*, 251, 288, doi: [10.1016/0370-2693\(90\)90938-3](https://doi.org/10.1016/0370-2693(90)90938-3)
- . 1991, *Nucl. Phys. B*, 363, 3, doi: [10.1016/0550-3213\(91\)90231-L](https://doi.org/10.1016/0550-3213(91)90231-L)
- Özel, F., & Freire, P. 2016, *Annual Review of Astronomy and Astrophysics*, 54, 401–440, doi: [10.1146/annurev-astro-081915-023322](https://doi.org/10.1146/annurev-astro-081915-023322)



## ACKNOWLEDGEMENTS

We thank Sumit Kumar, Sanjay Reddy, Ingo Tews, and Duncan Brown for their valuable discussions. Our computations used the ATLAS computing cluster at AEI Hannover [AEI \(2017\)](#) funded by the Max Planck Society and the State of Niedersachsen, Germany.

This research has made use of data, software, and/or web tools obtained from the LIGO Open Science Center (<https://losc.ligo.org>), a service of LIGO Laboratory, the LIGO Scientific Collaboration and the Virgo Collaboration. LIGO is funded by the U.S. National Science Foundation. Virgo is funded by the French Centre National de Recherche Scientifique (CNRS), the Italian Istituto Nazionale della Fisica Nucleare (INFN), and the Dutch Nikhef, with contributions by Polish and Hungarian institutes.

## APPENDIX

## A. DATA TABLES

**Table 1.** Neutron-Star–Black-Hole with LIGO-Virgo

90 <sup>th</sup> % Stiff				Maximum Likelihood			
Mass <sub>BH</sub> [ $M_{\odot}$ ]	Distance [Mpc]	SNR	$\log_e \mathcal{B}$	Mass <sub>BH</sub> [ $M_{\odot}$ ]	Distance [Mpc]	SNR	$\log_e \mathcal{B}$
5	40	139	0.8	5	40	139	0.7
10	40	168	0.5	10	40	168	0.7
15	40	180	0.3	15	40	180	0.3
20	40	190	0.3	20	40	190	0.3
5	80	69	0.4	5	80	69	0.1
10	80	84	0.2	10	80	84	0.1
15	80	90	0.3	15	80	90	0.4
20	80	95	0.4	20	80	95	0.4

**Table 2.** Neutron-Star–Black-Hole with LIGO-Virgo and equation of state held constant

90 <sup>th</sup> % Stiff				Maximum Likelihood			
Mass <sub>BH</sub> [ $M_{\odot}$ ]	Distance [Mpc]	SNR	$\log_e \mathcal{B}$	Mass <sub>BH</sub> [ $M_{\odot}$ ]	Distance [Mpc]	SNR	$\log_e \mathcal{B}$
5	40	139	0.8	5	40	139	0.8
10	40	168	0.4	10	40	168	0.3
15	40	180	-0.1	15	40	180	0.1
20	40	190	0.0	20	40	190	0.0
5	80	69	0.5	5	80	69	0.1
10	80	84	-0.2	10	80	84	-0.2
15	80	90	0.0	15	80	90	-0.1
20	80	95	0.1	20	80	95	0.2

**Table 3.** Neutron-Star-Black-Hole with LIGO A+

90 <sup>th</sup> % Stiff				Maximum Likelihood			
Mass <sub>BH</sub> [ $M_{\odot}$ ]	Distance [Mpc]	SNR	$\log_e \mathcal{B}$	Mass <sub>BH</sub> [ $M_{\odot}$ ]	Distance [Mpc]	SNR	$\log_e \mathcal{B}$
5	40	264	2.5	5	40	264	1.0
10	40	316	0.7	10	40	316	0.6
15	40	329	0.4	15	40	329	0.4
20	40	344	0.3	20	40	344	0.4
5	80	132	1.0	5	80	132	0.1
10	80	158	0.2	10	80	158	0.0
15	80	164	0.1	15	80	164	0.3
20	80	172	0.5	20	80	172	0.3

**Table 4.** Neutron-Star-Black-Hole with LIGO A+ with equation of state held constant

90 <sup>th</sup> % Stiff				Maximum Likelihood			
Mass <sub>BH</sub> [ $M_{\odot}$ ]	Distance [Mpc]	SNR	$\log_e \mathcal{B}$	Mass <sub>BH</sub> [ $M_{\odot}$ ]	Distance [Mpc]	SNR	$\log_e \mathcal{B}$
5	40	264	3.2	5	40	264	0.9
10	40	316	0.7	10	40	316	0.2
15	40	329	-0.2	15	40	329	-0.1
20	40	344	0.1	20	40	344	0.0
5	80	132	1.0	5	80	132	0.2
10	80	158	-0.3	10	80	158	-0.2
15	80	164	-0.1	15	80	164	0.1
20	80	172	0.1	20	80	172	0.1

**Table 5.** Neutron-Star-Black-Hole with LIGO Voyager

90 <sup>th</sup> % Stiff				Maximum Likelihood			
Mass <sub>BH</sub> [ $M_{\odot}$ ]	Distance [Mpc]	SNR	$\log_e \mathcal{B}$	Mass <sub>BH</sub> [ $M_{\odot}$ ]	Distance [Mpc]	SNR	$\log_e \mathcal{B}$
5	40	604	8.7	5	40	604	2.0
10	40	738	0.5	10	40	738	1.0
15	40	791	0.4	15	40	791	0.5
20	40	837	0.2	20	40	837	0.1
5	80	302	2.6	5	80	302	0.5
10	80	369	-0.4	10	80	369	-0.2
15	80	396	0.2	15	80	396	0.2
20	80	419	0.0	20	80	419	0.0

**Table 6.** Neutron-Star–Black-Hole with LIGO Voyager and equation of state held constant

90 <sup>th</sup> % Stiff				Maximum Likelihood			
Mass <sub>BH</sub> [ $M_{\odot}$ ]	Distance [Mpc]	SNR	$\log_e \mathcal{B}$	Mass <sub>BH</sub> [ $M_{\odot}$ ]	Distance [Mpc]	SNR	$\log_e \mathcal{B}$
5	40	604	9.5	5	40	604	2.4
10	40	738	1.6	10	40	738	0.7
15	40	791	-0.1	15	40	791	0.3
20	40	837	-0.1	20	40	837	0.1
5	80	302	2.8	5	80	302	0.5
10	80	369	-0.7	10	80	369	-0.3
15	80	396	-0.1	15	80	396	0.1
20	80	419	-0.1	20	80	419	0.0

**Table 7.** Neutron-Star–Black-Hole with Cosmic Explorer 1 40km

90 <sup>th</sup> % Stiff				Maximum Likelihood			
Mass <sub>BH</sub> [ $M_{\odot}$ ]	Distance [Mpc]	SNR	$\log_e \mathcal{B}$	Mass <sub>BH</sub> [ $M_{\odot}$ ]	Distance [Mpc]	SNR	$\log_e \mathcal{B}$
5	40	2888	94.0	5	40	2888	16.8
10	40	3617	1.9	10	40	3617	0.3
15	40	4055	0.5	15	40	4055	0.1
20	40	4390	0.1	20	40	4390	-0.1
5	80	1444	21.9	5	80	1444	3.1
10	80	1809	0.4	10	80	1809	-0.2
15	80	2028	0.5	15	80	2028	0.5
20	80	2195	0.3	20	80	2195	0.2

**Table 8.** Neutron-Star–Black-Hole with Cosmic Explorer 1 40km and equation of state held constant

90 <sup>th</sup> % Stiff				Maximum Likelihood			
Mass <sub>BH</sub> [ $M_{\odot}$ ]	Distance [Mpc]	SNR	$\log_e \mathcal{B}$	Mass <sub>BH</sub> [ $M_{\odot}$ ]	Distance [Mpc]	SNR	$\log_e \mathcal{B}$
5	40	2888	95.4	5	40	2888	17.7
10	40	3617	2.0	10	40	3617	0.4
15	40	4055	0.0	15	40	4055	-0.1
20	40	4390	-0.3	20	40	4390	-0.2
5	80	1444	22.5	5	80	1444	3.5
10	80	1809	0.1	10	80	1809	0.0
15	80	2028	0.5	15	80	2028	0.4
20	80	2195	0.3	20	80	2195	-0.1

**Table 9.** Neutron-Star–Black-Hole with Cosmic Explorer 2 40km

90 <sup>th</sup> % Stiff				Maximum Likelihood			
Mass <sub>BH</sub> [ $M_{\odot}$ ]	Distance [Mpc]	SNR	$\log_e \mathcal{B}$	Mass <sub>BH</sub> [ $M_{\odot}$ ]	Distance [Mpc]	SNR	$\log_e \mathcal{B}$
5	40	4385	210.3	5	40	4385	37.6
10	40	5491	3.6	10	40	5491	0.6
15	40	6151	0.7	15	40	6151	0.4
20	40	6655	0.2	20	40	6655	0.0
5	80	2193	50.5	5	80	2193	7.9
10	80	2745	1.2	10	80	2745	0.0
15	80	3075	0.8	15	80	3075	0.4
20	80	3328	0.3	20	80	3328	0.3

**Table 10.** Neutron-Star–Black-Hole with Cosmic Explorer 2 40km and equation of state held constant

90 <sup>th</sup> % Stiff				Maximum Likelihood			
Mass <sub>BH</sub> [ $M_{\odot}$ ]	Distance [Mpc]	SNR	$\log_e \mathcal{B}$	Mass <sub>BH</sub> [ $M_{\odot}$ ]	Distance [Mpc]	SNR	$\log_e \mathcal{B}$
5	40	4385	212.1	5	40	4385	38.8
10	40	5491	3.6	10	40	5491	0.3
15	40	6151	0.5	15	40	6151	0.2
20	40	6655	-0.3	20	40	6655	0.0
5	80	2193	51.3	5	80	2193	8.6
10	80	2745	1.2	10	80	2745	0.1
15	80	3075	0.6	15	80	3075	0.3
20	80	3328	0.1	20	80	3328	-0.2

**Table 11.** Log Bayes Factor and standard deviation for cases with  $M_{BH} = 5M_{\odot}$ .

$M_{BH}$ [ $M_{\odot}$ ]	d[Mpc]	EOS	A+	Voyager	CE1 (const)	CE1 (var)	CE2 (const)	CE2 (var)
5	40	stiff	$2.5 \pm 1.5$	$8.7 \pm 3.1$	$95.4 \pm 13.0$	$94.0 \pm 12.6$	$212.1 \pm 19.5$	$210.3 \pm 19.3$
5	40	soft	$1.0 \pm 1.1$	$2.0 \pm 1.6$	$17.7 \pm 5.0$	$16.8 \pm 4.8$	$38.8 \pm 7.3$	$37.6 \pm 7.1$
5	80	stiff	$1.0 \pm 0.8$	$2.6 \pm 2.0$	$22.5 \pm 9.4$	$21.9 \pm 8.0$	$51.3 \pm 13.9$	$50.5 \pm 12.6$
5	80	soft	$0.1 \pm 0.8$	$0.5 \pm 1.5$	$3.5 \pm 3.1$	$3.1 \pm 2.8$	$8.6 \pm 4.4$	$7.9 \pm 3.9$
10	40	stiff	$0.7 \pm 0.5$	$0.5 \pm 0.7$	$2.0 \pm 1.4$	$1.9 \pm 1.8$	$3.6 \pm 2.3$	$3.6 \pm 1.9$